

Rapid Decline of Total Antarctic Sea Ice Extent during 2014–16 Controlled by Wind-Driven Sea Ice Drift

ZHAOMIN WANG

College of Oceanography, and International Polar Environment Research Laboratory, Hohai University, Nanjing, and University Corporation for Polar Research, Beijing, China

JOHN TURNER

British Antarctic Survey, Cambridge, United Kingdom

YANG WU AND CHENGYAN LIU

College of Oceanography, and International Polar Environment Research Laboratory, Hohai University, Nanjing, and University Corporation for Polar Research, Beijing, China

(Manuscript received 24 September 2018, in final form 27 May 2019)

ABSTRACT


Between 2014 and 2016 the annual mean total extent of Antarctic sea ice decreased by a record, unprecedented amount of 1.6×10^6 km², the largest in a record starting in the late 1970s. The mechanisms behind such a rapid decrease remain unknown. Using the outputs of a high-resolution, global ocean–sea ice model we show that the change was predominantly a result of record atmospheric low pressure systems over sectors of the Southern Ocean in 2016, with the associated winds inducing strong sea ice drift. Regions of large positive and negative sea ice extent anomaly were generated by both thermal and dynamic effects of the wind anomalies. Although the strong wind forcing also generated the warmest ocean surface state from April to December 2016, we show that enhanced northward sea ice drift and hence increased melting at lower latitudes driven by strong winds made the dominant contribution to the large decrease in total Antarctic sea ice extent between 2014 and 2016.

1. Introduction

During 2014–16 Antarctic sea ice retreated at an unprecedented rate with total sea ice extent (SIE) reaching a record low level in spring 2016 (Fig. 1). This was unexpected, as there had been a small but significant upward trend in total Antarctic SIE since 1978 (Comiso and Nishio 2008; Turner et al. 2009; Parkinson and Cavalieri 2012), with record high daily extents being observed in September 2012 (Turner et al. 2013), 2013 (Reid et al. 2015), and 2014 (Fetterer et al. 2017; Massonnet et al. 2015). On 19 September 2014, Antarctic sea ice reached a record maximum extent of more

than 20 million square kilometers, the largest in a dataset starting in 1978 (Fetterer et al. 2017; Massonnet et al. 2015). Such a large decrease over the last several years in total Antarctic SIE shows another marked difference between the two polar regions, in addition to their contrasting trends over the past decades (Parkinson and Comiso 2013).

Regional Antarctic sea ice variability has been attributed to several aspects of atmospheric forcing associated with atmospheric planetary waves (Raphael 2007), the Amundsen Sea low (Hosking et al. 2013), the El Niño–Southern Oscillation cycle, and the southern annular mode (SAM) (Simmonds and Jacka 1995; Liu et al. 2004; Lefebvre and Goosse 2005; Simpkins et al. 2012; Wang et al. 2015; Kohyama and Hartmann 2016; Doddridge and Marshall 2017; Turner et al. 2017). Both atmospheric thermal effects (e.g., warm/cold air advection) and dynamic influences (e.g., wind-driven sea ice drift contributions) can cause large regional sea ice

 Denotes content that is immediately available upon publication as open access.

Corresponding author: Zhaomin Wang, zhaomin.wang@hhu.edu.cn

DOI: 10.1175/JCLI-D-18-0635.1

© 2019 American Meteorological Society. For information regarding reuse of this content and general copyright information, consult the [AMS Copyright Policy](https://www.ametsoc.org/PUBSReuseLicenses) (www.ametsoc.org/PUBSReuseLicenses).

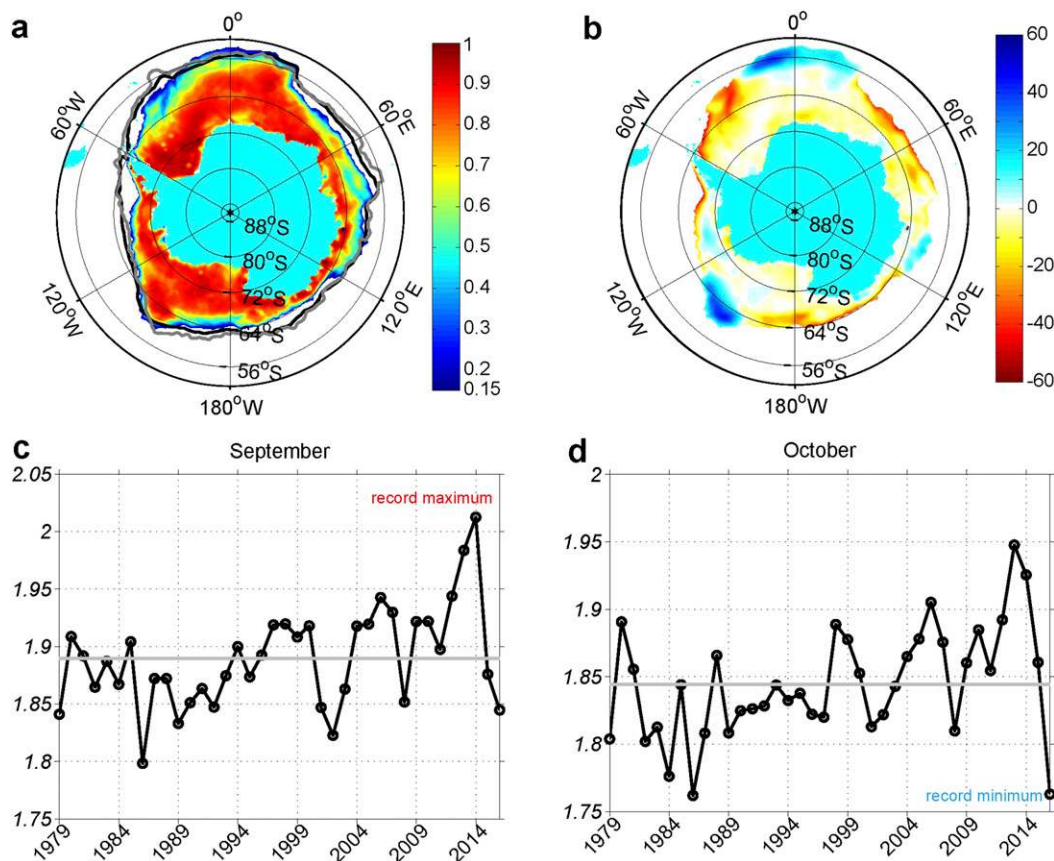


FIG. 1. (a) Sea ice concentration (>0.15) in October 2016. The black line and the gray line indicate the locations where the sea ice concentration is 0.15 for the mean over 1979–2015 and for 2014, respectively. (b) Sea ice concentration anomaly (relative to the mean over 1979–2015) in October 2016. (c) Monthly total Antarctic sea ice extent (10^7 km^2) in September from 1979 to 2016 (black line) and the mean over 1979–2015 in September. (d) As in (c), but for October.

variability. The ocean is also a key driver, as the mixed layer is directly involved in interactions between atmosphere, ocean, and sea ice. Some concepts and hypotheses have been developed or debated regarding oceanic processes that drive the variability in the mixed layer, and these are mainly related to sea ice–ocean feedback (Martinson 1990; Zhang 2007; GooSe and Zunz 2014; Venables and Meredith 2014) and the effects of surface buoyancy forcing (Marsland and Wolff 2001; Bintanja et al. 2013; Swart and Fyfe 2013; Haid et al. 2017). The persistence or re-emergence of ocean temperature anomalies can also lead to sea ice anomalies over periods of a few months or longer (Stammerjohn et al. 2012; Holland et al. 2013).

In particular, several studies have examined the characteristics of atmospheric and oceanic processes related to the large sea ice loss in spring 2016. Turner et al. (2017) found that sea ice in the Weddell Sea sector retreated rapidly in strong northerly flow after an early maximum extent on 28 August; in the Ross Sea sector,

rapid ice retreat took place in November when the SAM was at its most negative since 1968. Schlosser et al. (2018) found that strong meridional flow and anomalously strong southward heat advection in the regions of strongest sea ice decline existed from May to August, manifested by a persistently positive zonal wavenumber-3 index (Raphael 2007) during this period. They further suggested that the resulting decrease in sea ice concentration (SIC) between May and August preconditioned the SIE decrease in spring 2016. Wang et al. (2019) and Meehl et al. (2019) found that an extreme Indian Ocean dipole event characterized by a positive convective heating anomaly in the eastern Indian Ocean generated anomalous Rossby waves in spring 2016, contributing to the large decline of Antarctic SIE. Aside from these direct atmospheric thermal effects, it was suggested that the preceding strong El Niño event in December–February 2015/16 generated warm sea surface temperature (SST) anomalies within the eastern Ross and Amundsen Seas, and these

anomalies persisted strongly through November–December 2016 (Stuecker et al. 2017). The persistent warm anomalies were suggested to be due to the relatively weak La Niña and a pronounced negative SAM anomaly in November–December 2016. Meehl et al. (2019) even documented a decadal-scale warming trend in the upper Southern Ocean, and suggested that the sustained ocean warming also contributed to the large Antarctic sea ice decline in spring 2016. However, the relative roles of atmospheric and oceanic processes in driving the rapid decline in total Antarctic SIE during 2014–16 have not been assessed in a quantitative way, and hence the major driver has not been identified.

Here we have conducted a model-based and process-oriented study to identify the major driver for the rapid decline in total Antarctic SIE during 2014–16. We show that atmospheric dynamic effects (i.e., wind-driven effects on sea ice drift) played a more important role in controlling the unprecedented decrease of total Antarctic SIE during 2014–16 than atmospheric and oceanic thermal effects, in addition to driving regional SIC anomalies (Goosse et al. 2009; Holland and Kwok 2012). Advances in the production of atmospheric reanalysis, as well as great improvements in high-resolution ocean–sea ice modeling, facilitate quantifying the roles played by different forcing factors in generating the large decrease in total Antarctic SIE during 2014–16.

The paper is organized as follows. We begin in section 2 by describing the SIC data, reanalysis products, and the high-resolution global ocean–sea ice model used in this study. In section 3, we first examine the features of evolutions of observed and simulated monthly Antarctic SIE and sea ice area (SIA), and this is followed by a further investigation of the unusual atmospheric forcing conditions in 2016. Then, the dynamic effect of atmospheric forcing on regional SIC is examined and the dominant role of wind-driven sea ice drift in the rapid decline of total Antarctic SIE is demonstrated by conducting ensemble sensitivity experiments. Finally, section 4 provides a summary and some concluding remarks.

2. Data and methods

a. Sea ice and SST data

Daily SIC data were obtained from the U.S. National Snow and Ice Data Center (http://nsidc.org/data/seaice_index). Before 1987 SIC data are only available every other day. Monthly SIC data are derived from these data. As there were no satellite data during the latter half of December 1987 and the first half of January 1988, these two months were not included in our analysis. The sea ice data produced by the NASA Team algorithm 1.1

(Cavalieri et al. 1984) were used since these data are consistent during the period 1979–2016. SIE is defined as the sum of the area of each grid box where SIC is greater than 15% over a specified region. SIA is defined as the sum of the SIC at each grid box times the area of the grid box over a specified region.

SST data were obtained from NOAA Optimum Interpolation Sea Surface Temperature V2 (OISST V2) (Reynolds et al. 2002; <https://www.esrl.noaa.gov/psd/data/gridded/data.noaa.oisst.v2.html>).

b. Reanalysis products

Sea level pressure (SLP) data are from the European Centre for Medium-Range Weather Forecasts (ECMWF) interim reanalysis (ERA-Interim, hereafter ERA-I) fields (<https://www.ecmwf.int>), and from National Centers for Environmental Prediction (NCEP) reanalysis fields (NCEP2) (<https://www.esrl.noaa.gov/psd/>). ERA-I data (Dee et al. 2011) were interpolated onto a $0.75^\circ \times 0.75^\circ$ grid, and NCEP2 data (Kanamitsu et al. 2002) were interpolated onto $2.5^\circ \times 2.5^\circ$ grid from T62 Gaussian grid (192×64). A previous assessment (Bracegirdle and Marshall 2012) suggests that the ERA-I reanalysis data are more reliable than other reanalysis datasets at southern high latitudes. Here, both ERA-I and NCEP2 SLP data are analyzed to depict changes in atmospheric circulation at southern high latitudes.

c. The model

We used the MIT general circulation model (MITgcm) (Marshall et al. 1997a,b) in the state estimate configuration Estimating the Circulation and Climate of the Ocean, phase 2 (MITgcm-ECCO2) (Menemenlis et al. 2008), high-resolution global ocean and sea ice data synthesis. This state-of-the-art high-resolution global ocean–sea ice model has a cube-sphere grid configuration that has a relatively even grid spacing throughout the global ocean to avoid polar singularities (Adcroft et al. 2004). The mean horizontal grid size is about 18 km, and it has 50 vertical levels, with intervals ranging from 10 m near the surface to 450 m at the bottom. This ocean component is coupled with a sea ice model (Losch et al. 2010). The coupled ocean–sea ice model was run forward from 1979 to 2016 using optimized control parameters derived by Menemenlis et al. (2008) that were obtained through reducing model–data misfit by using the Green function approach [for details see Menemenlis et al. (2008)]. The model was forced by the 6-hourly variables obtained from ERA-I dataset, including 6-hourly net downward longwave and shortwave radiation, 2-m humidity, 2-m air temperature, 10-m surface winds, and precipitation. This experiment is defined as our control run.

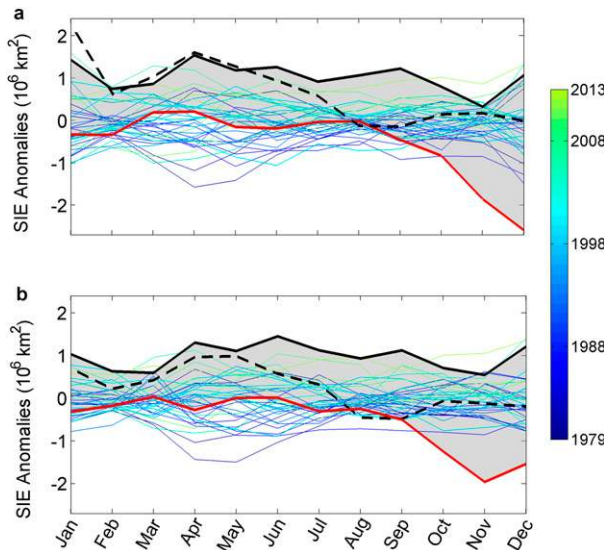


FIG. 2. Observed and simulated monthly total Antarctic SIE anomalies. The model well captured the salient features in the observed Antarctic sea ice annual cycles and large decrease between 2014 and 2016. (a) Observed monthly total Antarctic SIE anomalies (relative to the mean over 1979–2015) for each year from 1979 to 2013 (see the color bar on the right side), in 2014 (black solid), in 2015 (black dashed), and in 2016 (red solid). (b) Simulated monthly total Antarctic SIE anomalies for each year from 1979 to 2013, in 2014 (black solid), in 2015 (black dashed), and in 2016 (red solid). The shading in light gray highlights the large decrease in total Antarctic sea ice extent between 2014 and 2016.

3. Results

a. Observed and simulated monthly Antarctic SIE and SIA

Monthly total Antarctic SIE anomalies (relative to their climatological monthly means over 1979–2015; hereafter, anomalies are calculated in the same way for other variables if not specified) showed large decrease between 2014 and 2016 (Fig. 2a). Throughout the year 2014, the monthly total Antarctic SIEs reached very high or even record high values, with the annual mean value ($13.14 \times 10^6 \text{ km}^2$) (obtained by averaging daily values) being the largest value in the dataset starting in 1978. After June 2015 the monthly total SIE started to fall and approached the means for 1979–2015 between August 2015 and August 2016. From September 2016, the total Antarctic SIEs declined dramatically and reached record low values in October, November, and December 2016. These salient features were well captured by the MITgcm-ECCO2 (Fig. 2b). The correlation coefficients between the observed and simulated monthly SIE anomalies are 0.85 (confidence level greater than 99% by the Monte Carlo method) over 1979–2016 and 0.91 (confidence level greater than 99%

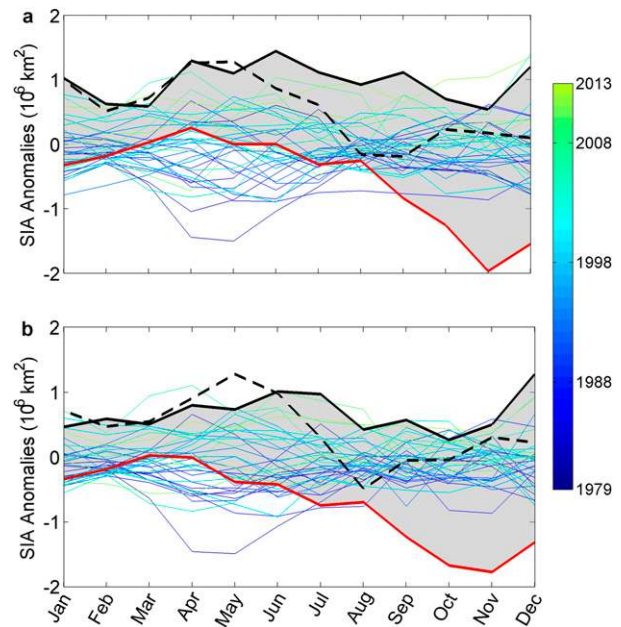


FIG. 3. As in Fig. 2, but for total Antarctic SIA anomalies.

by the Monte Carlo method) over 2014–16, with the root-mean-square errors being $0.29 \times 10^6 \text{ km}^2$ over 1979–2016 and $0.12 \times 10^6 \text{ km}^2$ over 2014–16.

The monthly total SIA anomalies evolved in a similar way to the total SIE anomalies between 2014 and 2016 (Fig. 3). However, in contrast, both the observed and simulated total SIA anomalies started to decline monotonically from April 2016, and reached record low values in September 2016, one month earlier than the timing of the first record low monthly total SIE in 2016. Although the model also captured the salient features in the observed SIA evolution, the simulated total SIA anomaly declined at a slightly faster rate and reached a lower anomaly ($-1.23 \times 10^6 \text{ km}^2$) than the observed ($-0.84 \times 10^6 \text{ km}^2$) in September 2016. It is not clear if this is owing to a slightly more sensitive model response to atmospheric and oceanic forcing in 2016, or owing to the less accurate SIC satellite product as there are potential inaccuracies in the observed SIC, particularly during the melt phase. As the total SIA is an area integral of SIC over the whole sea ice–covered region, the differences between the total SIE and SIA evolutions in 2016 reflect more detailed changes in sea ice cover. Thus, the analysis of total SIA is useful for revealing the effects of atmospheric and oceanic forcing (see below) in much earlier time in 2016 that cannot be seen in the total SIE analysis.

The monthly SIE evolutions over five sectors are further examined in Fig. 4. Following Zwally et al. (2002) and Turner et al. (2017), these five sectors are

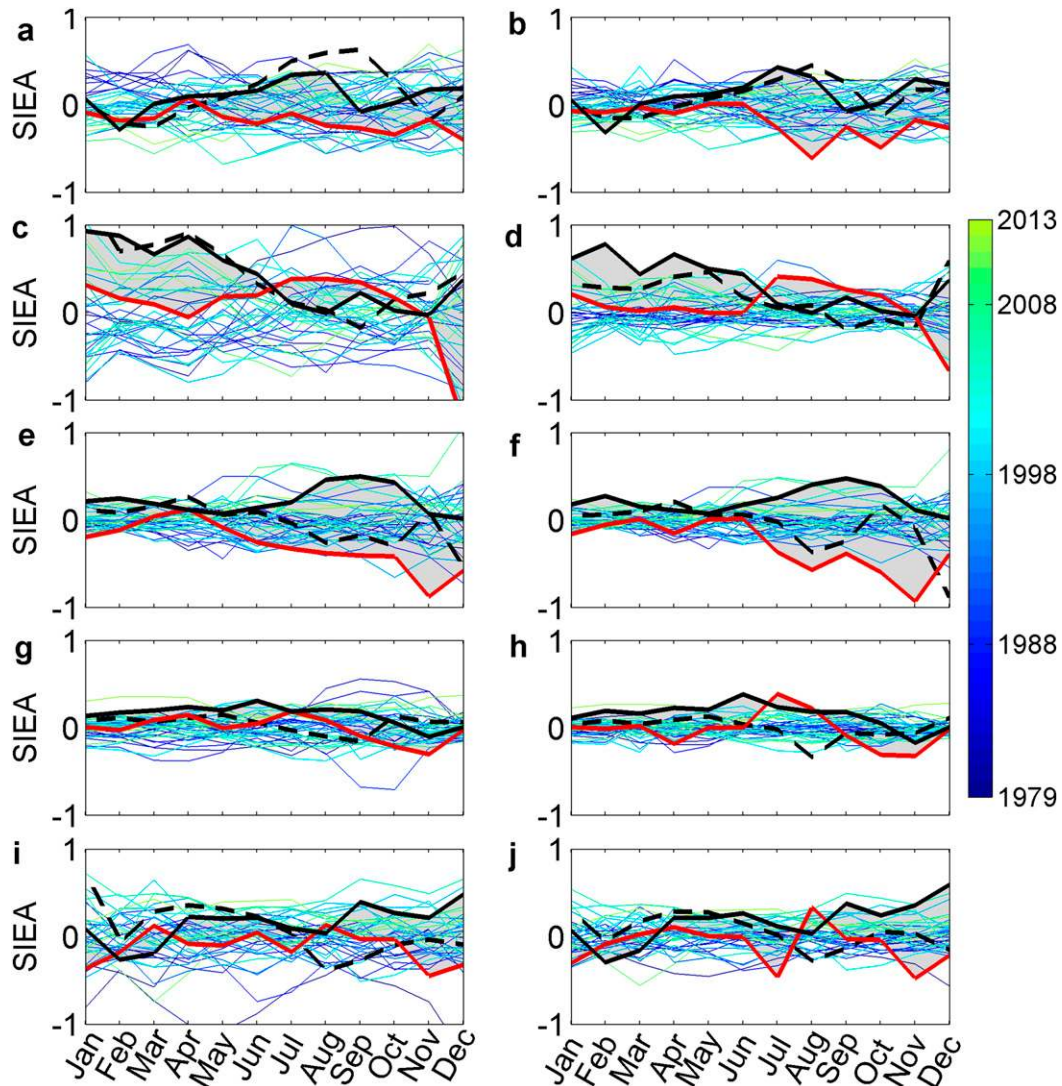


FIG. 4. As in Fig. 2, but for SIE anomalies (10^6 km^2) over the five sectors for (left) observed and (right) simulated: (a),(b) the Ross Sea (160°E – 130°W); (c),(d) Amundsen-Bellingshausen Sea (130° – 60°W); (e),(f) Weddell Sea (60°W – 20°E); (g),(h) Indian Ocean (20° – 90°E); and (i),(j) western Pacific Ocean (90° – 160°E).

selected as the Ross Sea (160°E – 130°W), Amundsen-Bellingshausen Sea (130° – 60°W), Weddell Sea (60°W – 20°E), Indian Ocean (20° – 90°E), and western Pacific Ocean (90° – 160°E). Regional differences of monthly SIE evolutions for 2014–16 are quite significant; in particular, opposite month-to-month changes are observed between the Ross Sea (Fig. 4a) and Amundsen-Bellingshausen Sea (Fig. 4c), as also revealed by, for example, Turner et al. (2009). The record maximum total SIE in September 2014 was mainly attributed to the record maximum SIE in the Weddell Sea (Fig. 4e) and the very large SIE anomalies in the western Pacific Ocean (Fig. 4i) and Indian Ocean (Fig. 4g). The record minimum total SIE in October 2016 was mainly

attributed to the large declines in the Ross Sea (Fig. 4a), Weddell Sea (Fig. 4e), and Indian Ocean (Fig. 4g), but the subsequent further drop over October–December 2016 was mainly induced by the SIE reductions in the Amundsen-Bellingshausen Sea (Fig. 4c), Weddell Sea (Fig. 4e), and western Pacific Ocean (Fig. 4i). These major features were well simulated by the model, despite that some more detailed features could not be captured (e.g., the model produced some smaller interannual variability).

b. Extreme atmospheric forcing conditions in 2016

In addition to the analysis of atmospheric forcing conditions in 2016 in Turner et al. (2017), Schlosser et al. (2018),

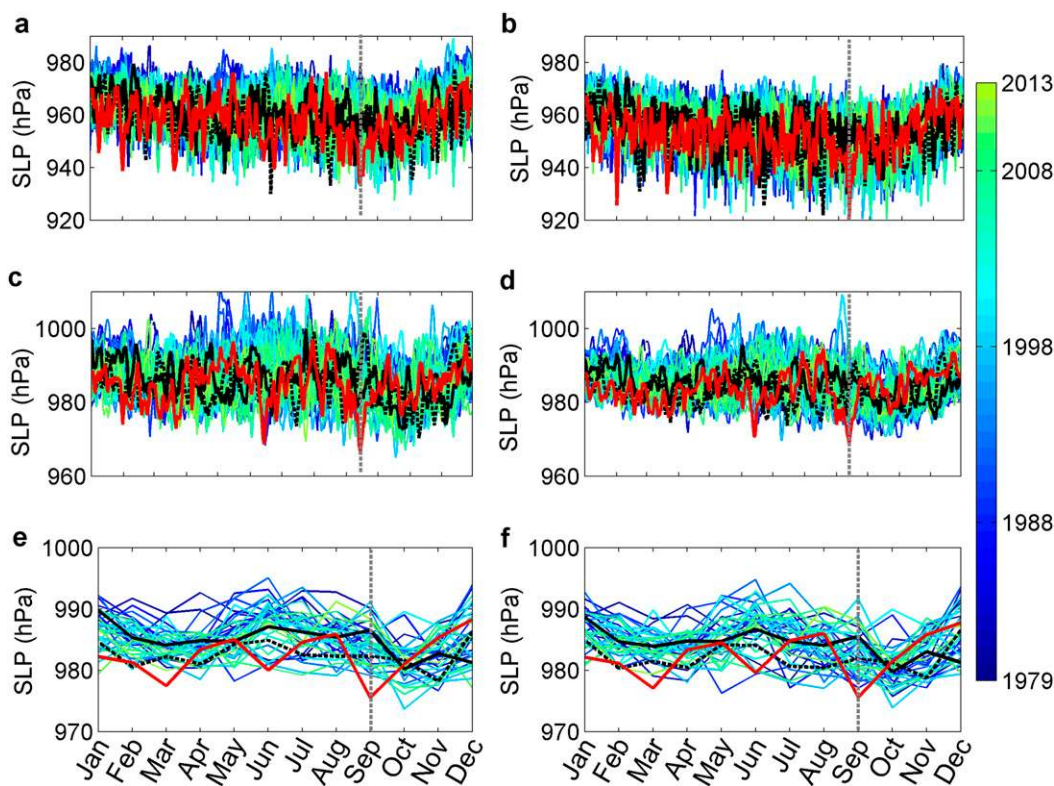


FIG. 5. Daily and monthly mean SLP for 1979–2016. Extreme atmospheric conditions in 2016 were characterized by a number of extreme and record low daily and monthly mean SLP at southern high latitudes. (a) Minimum daily SLP to the south of 55°S derived from NCEP2. (b) As in (a), but derived from ERA-I. (c) Average daily SLP over 60°–70°S derived from NCEP2. (d) As in (c), but derived from ERA-I. (e) Minimum monthly SLP to the south of 55°S derived from NCEP2. (f) As in (e), but derived from ERA-I. The black solid lines are for 2014, black dashed lines for 2015, red solid lines for 2016, and other lines for each year from 1979 to 2013 (see the color bar on the right side).

Wang et al. (2019), and Meehl et al. (2019), we here further document extreme atmospheric forcing conditions reflected by extreme SLP anomalies at southern high latitudes in 2016. From the beginning of 2016, minimum daily SLP to the south of 55°S reached or was very close to record low values on several occasions (Figs. 5a,b; Table 1). Because of the finer model resolution, a much lower extreme daily SLP value was captured in ERA-I (925.7 hPa) compared to NCEP2 (938.8 hPa) on 1 February and in ERA-I on 11 September 2016 (920.1 hPa) than in NCEP2 on 13 September (933.6 hPa), and there are generally lower record low values in ERA-I than in NCEP2. These record low daily SLP values reflect extremely strong storm activities at southern high latitudes in 2016.

These extreme atmospheric conditions in 2016 also occurred alongside extremely low average daily SLP over the circumpolar trough region (60°–70°S) (Figs. 5c,d; Table 2). Note that the extreme low values of the average SLP over 60°–70°S in ERA-I are generally close to those in NCEP2 (Table 2), despite the fact that minimum values of daily SLP to the south of 55°S were very different in the two reanalysis datasets (Table 1), as expected by the spatial averaging process if higher resolution is responsible for the lower minima in ERA-I.

On the monthly scale, extremely strong atmospheric wind forcing was identified in 2016, as reflected in record low monthly mean SLP, clearly in March (NCEP2: 977.4 hPa; ERA-I: 977.1 hPa), June (NCEP2: 980.0 hPa;

TABLE 1. Extremely low daily sea level pressure values to the south of 55°S in 2016.

NCEP2	9 Jan, 945.7 hPa	1 Feb, 938.8 hPa	21 Mar, 938.8 hPa	25 Jun, 939.4 hPa	14 Sep, 933.6 hPa
ERA-I	16 Jan, 941.7 hPa	1 Feb, 925.7 hPa	21 Mar, 938.8 hPa	14 Jun, 933.4 hPa	11 Sep, 920.1 hPa

TABLE 2. Extremely low average daily sea level pressure values over the circumpolar trough region (60°–70°S) in 2016.

NCEP2	31 Jan, 974.0 hPa	22 Mar, 972.9 hPa	15 Jun, 968.7 hPa	14 Sep, 965.9 hPa	
ERA-I	31 Jan, 978.9 hPa	19 Feb, 976.6 hPa	12 Mar, 976.2 hPa	14 Jun, 970.5 hPa	13 Sep, 968.6 hPa

ERA-I: 979.6 hPa), and September (NCEP2: 975.5 hPa; ERA-I: 975.6 hPa) (Figs. 5e,f). In addition to the record low pressure in these months, the monthly SLP was also very close to record low values in January and February 2016 in both NCEP2 and ERA-I, indicating particularly persistent extreme atmospheric conditions during the first three months of 2016.

We note that there is no a clear linear relationship between the minimum monthly mean SLP in Fig. 5f and the total SIE in Fig. 2a, which is consistent with the result in Godfred-Spenning and Simmonds (1996). This result suggests that large variability in total SIE is usually not generated by atmospheric forcing in a single month.

These very low or even record low monthly SLPs were mainly associated with a very deep Amundsen Sea low (see the first column of Fig. 6), except for the case in January 2016; in addition, these very low monthly SLPs reflect a stronger zonal wavenumber-3 pattern in March and June 2016. The persistently strong zonal wavenumber-3 pattern was also found to exist from May to August 2016 (Schlosser et al. 2018). Along with the most negative SAM in November since 1968 (Turner et al. 2017), these results indicate that the large-scale meridional flow and cyclonic wind forcing at southern high latitudes were severely strong and persistent since the beginning of 2016. The persistently strong cyclonic wind forcing generated extremely strong Ekman pumping at a number of places in January (Fig. 6b), February (Fig. 6f), March (Fig. 6j), June (Fig. 6n), and September (Fig. 6r) 2016. The strong Ekman pumping brought warm water to the surface, contributing to the warm anomalies at surface that were particularly clear in March (Fig. 6k), June (Fig. 6o), and September (Fig. 6s) 2016.

We note that there exist some biases in the simulated SSTs, particularly in January 2016 (see the fourth column of Fig. 6). Without assimilating observed ocean temperature and salinity, the deficiencies in the state-of-the-art ocean general circulation models and atmospheric forcing data are prone to generate biased results. These biases apparently influence the simulated sea ice circulation, particularly over a long-term period. However, the well captured evolutions of monthly SIE and SIA anomalies, as shown in Figs. 2 and 3, suggest that the effects of these biases on the simulated large sea ice variability between 2014 and 2016 are rather weak. Despite the cold biases at the beginning of 2016, the model captured the significant surface warming since

March 2016 in response to extremely strong Ekman pumping during the first three months of 2016. Meehl et al. (2019) suggested that the ocean warming also contributed to the large Antarctic sea ice decline in spring 2016. It is, therefore, worth of quantifying the role of such ocean surface warming in driving the large decline in total SIE in spring 2016 (see below).

In addition to the Ekman pumping effect on the SST, these extreme atmospheric circulations generated strong surface winds and hence strong sea ice drifts. Below, the wind-driven sea ice drift effects on SIE and SIA were analyzed.

c. Atmospheric dynamic effect on regional SIC

To examine how sea ice responds to atmospheric forcing, we analyzed anomalies (relative to their corresponding monthly means over 1979–2015) of monthly mean SIC, 10-m winds, and sea ice velocity in June and September 2016 (Fig. 7). As illustrated by the black arrows (wind speeds and sea ice drift speeds above the 90th percentile of the corresponding monthly values from 1979 to 2016; no such extreme SIC anomalies were found, even though the monthly total SIA anomaly in September 2016 was record low) in Figs. 7a–d, the extreme atmospheric circulations generated very strong surface winds and sea ice drifts, particularly in September 2016. The simulated patterns of SIC anomalies in June 2016 (Fig. 7b) and in September 2016 (Fig. 7d) are in excellent agreement with the observed anomalies in June (Fig. 7a) and September (Fig. 7c) of 2016 (the spatial correlation coefficients between SIC anomalies in Figs. 7a and 7b and between SIC anomalies in Figs. 7c and 7d are 0.43 and 0.87, respectively, with the confidence level being greater than 99% by the Monte Carlo method), despite the fact that the magnitudes of the simulated SIC anomalies are smaller than the observed. The smaller magnitudes of the simulated SIC anomalies reflect some weaknesses in the model's representations of sea ice dynamic and thermodynamic processes and in the atmospheric forcing data, which need to be further investigated. Nonetheless, the model results have been encouraging enough to merit further investigation on what drive the large variability in total SIE and SIA.

Some positive and negative SIC anomalies have been suggested to be controlled by the atmospheric thermal effects (Turner et al. 2017), as warm (cold) air advection can lead to reduced (increased) SIC. The thermal effects

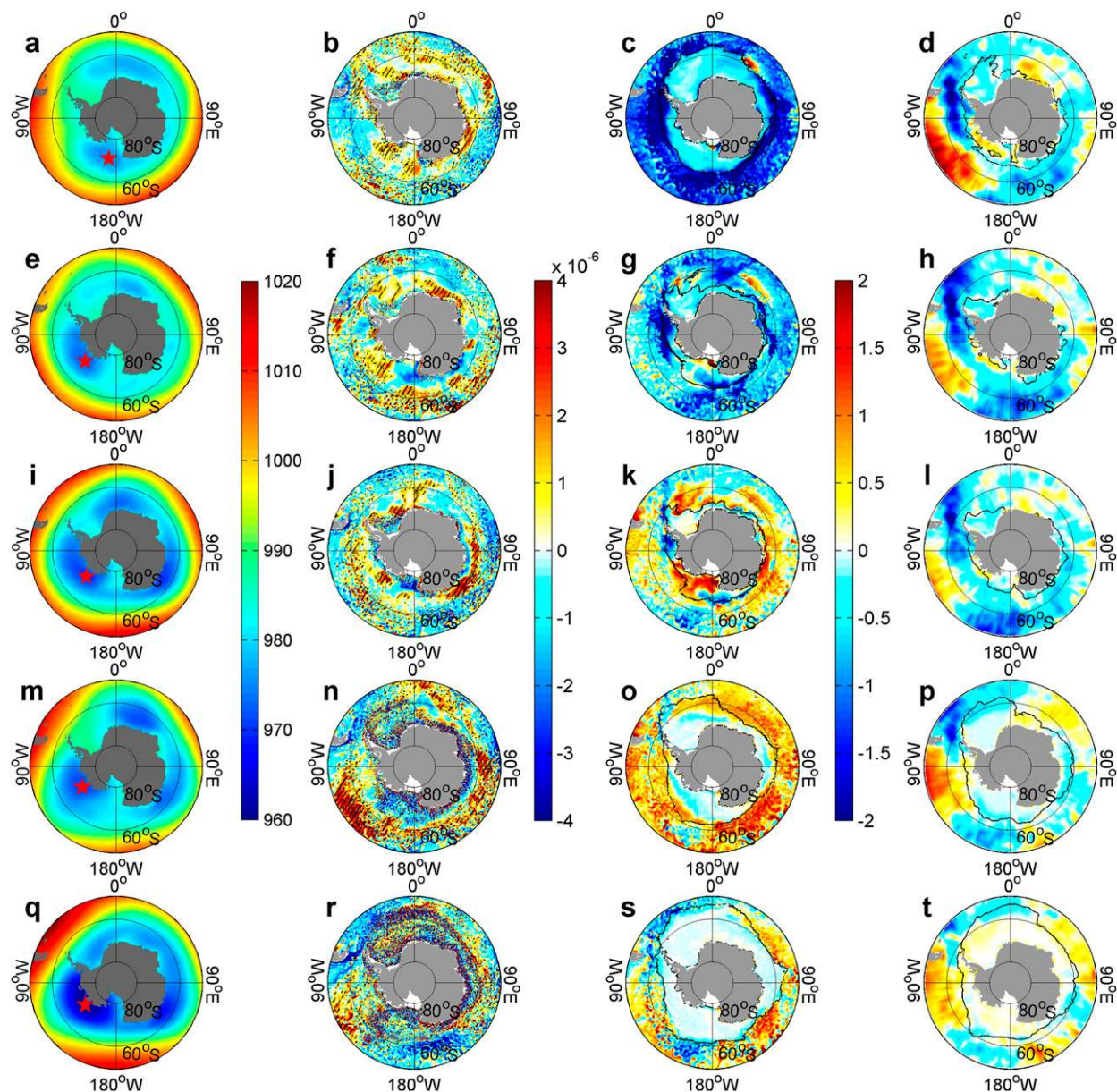


FIG. 6. (first column) Patterns of monthly mean SLP (hPa) from ERA-I in 2016 for (a) January; (e) February; (i) March; (m) June; and (q) September. The red stars mark the locations of the lowest monthly mean SLP to the south of 55°S in Fig. 5. (second column) Anomalies of monthly mean Ekman pumping vertical velocity (m s^{-1}) in 2016, calculated by using 10-m winds from ERA-I for (b) January; (f) February; (j) March; (n) June; and (r) September, with the values above the 90th percentile of the corresponding monthly values from 1979 to 2016 being shaded. (third column) Anomalies of monthly mean SST ($^{\circ}\text{C}$) simulated by MITgcm-ECCO2 in 2016 for (c) January; (g) February; (k) March; (o) June; and (s) September. (fourth column) Anomalies of monthly mean SST ($^{\circ}\text{C}$) (relative to their means over 1982–2015) derived from OISST V2 in 2016 for (d) January; (h) February; (l) March; (p) June; and (t) September. The gray lines mark the simulated (in the third column) and observed (in the fourth column) sea ice edge where SIC is 15%. The Ekman pumping vertical velocity is calculated by $w_e = \text{curl}_z(\tau/\rho f)$, where τ is wind stress, ρ is sea surface water density, and f is the Coriolis parameter.

are especially evident in the regions where sea ice variability is predominantly controlled by thermodynamic rather than dynamic processes, such as the Bellingshausen Sea, a region susceptible to advection of warm air (Kimura and Wakatsuchi 2011).

However, the dynamic effects of atmospheric forcing (i.e., the wind-driven sea ice drift effects) also caused large SIC anomalies. In the Southern Hemisphere, sea ice drift is deflected to the left of the surface wind direction. Using satellite-derived daily sea ice motion

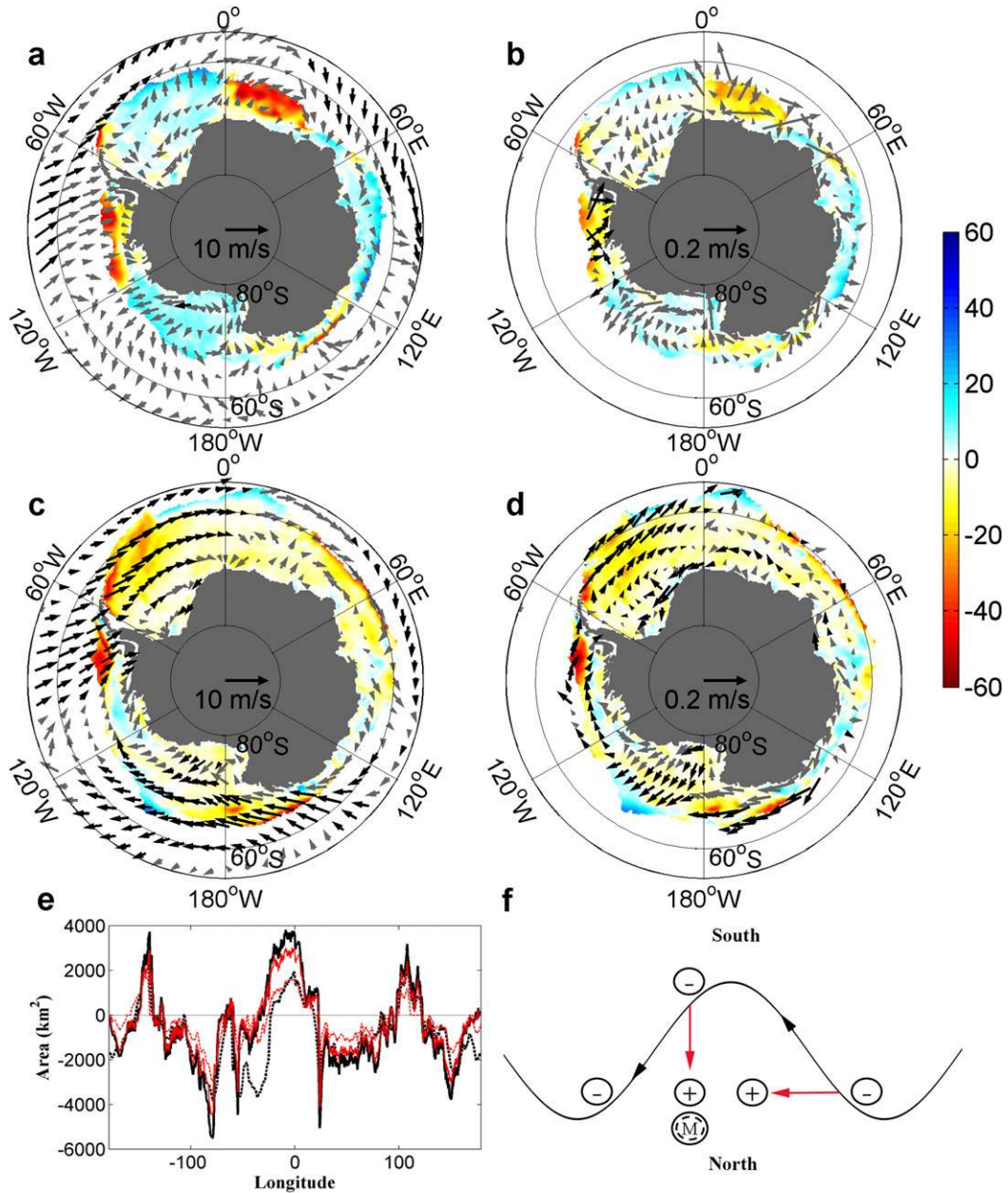


FIG. 7. Observed SIC and wind anomalies and simulated SIC and sea ice drift anomalies in June and September 2016. The wind-driven sea ice drift effect leads to substantial SIC anomalies. (a) Observed monthly wind (vectors; black arrows highlight the wind speeds above the 90th percentile of the corresponding monthly means from 1979 to 2016) and SIC anomalies in June 2016. (b) Simulated monthly sea ice velocity (vectors; black arrows highlight the sea ice drift speeds above the 90th percentile of the corresponding monthly means from 1979 to 2016; no such extreme SIC anomalies were found, even though the monthly total SIA anomaly in September 2016 was record low) and SIC anomalies in June 2016. (c) As in (a), but for September 2016. (d) As in (b), but for September 2016. (e) SIE and SIA anomalies integrated in the meridional direction over all sea ice covered grids within every longitudinal interval of 1° in September 2016 (black solid: observed SIE; black dashed: observed SIA; red solid: simulated SIE; red dashed: simulated SIA). (f) Schematic of wind-driven sea ice drift effects on SIC, with black arrows indicating wind anomalies, red ones indicating sea ice drift anomalies, “+” and “-” indicating positive and negative SIC anomaly, respectively, induced only by sea ice drift anomalies, and “M” standing for “melting” at lower latitudes.

data, Kimura (2004) obtained average turning angles over 1992–2001 of 10° – 20° in most of the Atlantic and Pacific sectors and of more than 30° in the coastal regions of the Indian sector. When sea ice internal stress is weak, the turning angle can be as large as 40° (Kottmeier et al. 1992; Wang et al. 2014). These results indicate that the turning angle is very variable. Here, our calculation indicates that the anomalous turning angles (the angles between anomalous wind directions and anomalous sea ice drift directions) can be up to 45° (not shown), as illustrated by the wind anomalies (Fig. 7c) and the northward sea ice drift anomalies around 150° W in September 2016 (Fig. 7d). In the other regions, the sea ice drift anomalies also clearly have a northward component (see Figs. 7b and 7d), although the anomalous turning angles might be smaller. This dynamical relationship results in anomalous sea ice drift being more northward than the anomalous winds when the cold air flows over sea ice from the southwest. The enhanced northward sea ice drift thus transports more sea ice away from the regions affected by cold advection and offsets the atmospheric thermal effects, leading to either smaller SIC increases (e.g., around 140° W in June 2016; Fig. 7b) or even SIC decreases (e.g., around 150° W in September 2016; Fig. 7d). As such, sea ice is being advected into a more northerly, warmer region.

Moreover, we note that the enhanced northward sea ice drift could also contribute to making negative SIC anomalies downstream (to the east of the regions with the enhanced northward sea ice drifts where the sea ice drift is largely eastward) by reduced eastward sea ice transport, together with the effects of the anomalies in previous months (Stammerjohn et al. 2008, 2012; Holland et al. 2013; Holland 2014). For instance, the negative SIC anomalies to the east of the prime meridian in Fig. 7b and the negative anomalies around 120° W in Figs. 7b and 7d lay to the east of the regions with enhanced northward sea ice transports. Our sensitivity experiment, in which the atmospheric forcing data in August 2016 were repeated for one more month to replace the forcing data in September 2016 to force the model, shows that the SIC anomalies in September 2016 (Fig. 7d) are largely created by the atmospheric forcing in September 2016 (not shown). Therefore, the dynamical effect of anomalous sea ice motion could also be used to explain some large SIC anomalies that could not be simply explained by the instantaneous thermal effects of warm or cold advection.

The wind-driven sea ice drift effects may also be invoked to explain the feature that the magnitudes of SIA anomalies are generally smaller than those of SIE anomalies for both the observed and the simulated results (Fig. 7e), in addition to thermodynamic effects.

Owing to the faster response of sea ice to dynamic forcing than to thermodynamic forcing, the dynamic effect tends to cause a larger change in SIE than in SIA by reducing interior SIC when sea ice is pushed northward and by increasing interior SIC when sea ice is pushed southward. We suggest that this dynamic effect was also responsible for the earlier occurrence of record low total SIA than that of record low total SIE (see Figs. 2 and 3) and contributed significantly to the subsequent large decline in total SIE in October 2016.

As a summary, the major dynamic effects of anomalous sea ice drifts driven by anomalous winds, without considering the thermodynamic effects here, are illustrated in Fig. 7f: anomalous winds from the southwest, corresponding to cold advection, generate northward sea ice drift anomalies, leading to the reduced SIC at higher latitudes and to the east of these sea ice drift anomalies, and increased SIC and melting at lower latitudes; anomalous winds from the northwest, corresponding to warm advection, generate eastward sea ice drift anomalies, leading to the reduced SIC to the west and the increased SIC to the east of these sea ice drift anomalies. During the melting season, large anomalous northward sea ice drifts could significantly contribute to a rapid decrease in total SIE, as demonstrated below.

d. Dominant wind-driven sea ice drift effect on total SIE

In this section, we show that the dynamic effect of wind-driven sea ice drift on SIC (Fig. 7) is mainly responsible for the large decline in total Antarctic SIE during 2014–16. This can be demonstrated by conducting three kinds of ensemble sensitivity experiments aimed at separating the atmospheric and oceanic roles from each other. In these ensemble experiments with 10 ensemble members for each year from 2006 to 2015, we quantify the roles played by the oceanic thermal forcing and atmospheric forcing in 2016, and also separate the dynamic and thermal effects of atmospheric forcing in 2016, in determining the large decline in total Antarctic SIE in spring 2016 (Table 3), similar to the approach used in Guemas et al. (2013), Massonnet et al. (2015), and Kushahara et al. (2018).

In experiment CTRL, which has only one member and 1-yr output for 2016, the results were simply taken from the output for 2016 from the control run defined in section 2c. In experiment 2016SST, which has 10 ensemble members corresponding to each year from 2006 to 2015, we replaced the daily SSTs in the sea ice module in every year from 2006 to 2015 by the daily SSTs in 2016 derived from the control run (defined in section 2c) and kept the atmospheric forcing from 2006 to 2015; in experiment 2016ATMOS (10 ensemble members), we

TABLE 3. Ensemble sensitivity experiments. Their ensemble annual mean total SIE anomalies relative to the annual mean over 2006–15 and standard deviations (10^5 km^2) are also given. See text for the explanation of each experiment.

Experiment	Year of atmospheric thermal forcing	Year of atmospheric dynamic forcing	Year of SST forcing	SIE anomaly
CTRL	2016	2016	2016	-8.6
2016ATMOS	2016	2016	2006–15	-6.2 ± 1.6
2016SST	2006–15	2006–15	2016	-1.4 ± 0.5
2016WINDS	2006–15	2016	2006–15	-5.7 ± 1.5

used the atmospheric forcing in 2016 and daily SSTs in every year from 2006 to 2015 from the control run to force the sea ice component; and in experiment 2016WINDS (10 ensemble members), we used the 10-m winds in 2016, other atmospheric forcing variables (net downward longwave and shortwave radiation, 2-m humidity, 2-m air temperature, and precipitation) and daily SSTs in every year from 2006–15 from the control run, to force the sea ice component. In these sensitivity experiments, the same initial conditions as in the control run were used (i.e., the conditions at the very beginning of 2006 in the control run) in order to compare the results from these sensitivity experiments with those from the control run. The ensemble means of monthly total SIE anomalies (relative to the monthly means over 2006–15) and their standard deviations from these sensitivity experiments are shown in Fig. 8a, along with the monthly SIE differences between 2016 and the means over 2006–15.

Although this approach was employed in some earlier studies (Guemas et al. 2013; Massonnet et al. 2015; Kushahara et al. 2018), we note that in these sensitivity experiments, atmospheric and oceanic states are not in dynamic and thermodynamic balance. The major inconsistency in such experiments is that the atmospheric and oceanic thermal conditions are not consistent with the wind directions. For instance, in a region affected by cold advection induced by winds from the southwest, if we just used the winds but no other thermal variables, it would be possible that the winds drive sea ice northward in a warmer condition. Consequently, less sea ice would be transported northward owing to reduced sea ice in a warmer condition. Similarly, in a region with winds from the northwest and a cold condition, more sea ice could be transported eastward. Reduced northward sea ice transport would likely lead to underestimated sea ice melt at lower latitudes and could hence affect the total SIE to some extent. However, these effects are likely small, as the sea ice response to atmospheric thermal forcing is much slower than the response to dynamic forcing, and the sea ice volume anomalies are generally within 10%–20% of mean values (not shown). Therefore, this is a useful approach for identifying major drivers of large sea ice variability.

We also note that major oceanic changes near the surface are also generated directly by atmospheric forcing. By prescribing the daily SSTs in the above experiments, we are able to isolate the effects of direct atmospheric forcing on sea ice from those of oceanic

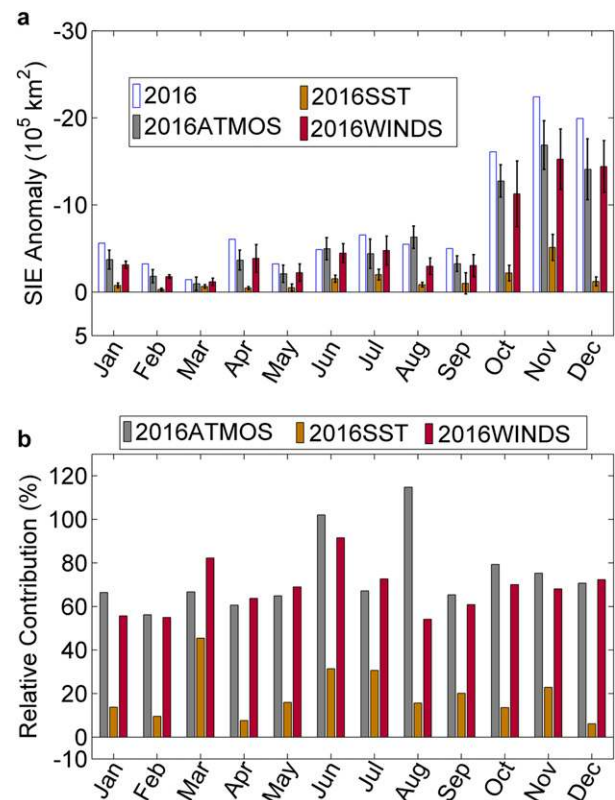


FIG. 8. Reductions in total Antarctic SIE generated by atmospheric and oceanic drivers. The effects of the wind-driven sea ice drift in 2016 explained the most differences in total sea ice extent between 2016 and the monthly means over 2006–15. (a) Monthly total sea ice extent differences between those ensemble means from the three sensitivity experiments (2016SST, 2016ATMOS, and 2016WINDS; see Table 3 and following text for how to design these experiments) and the means over 2006–15. The two standard deviations are given by the black vertical lines to show the SIE variability within the ensemble members. (b) Relative contributions of sea surface temperature forcing, full atmospheric forcing, and wind-only forcing in 2016 to the differences between monthly total sea ice extents in 2016 and the means over 2006–15.

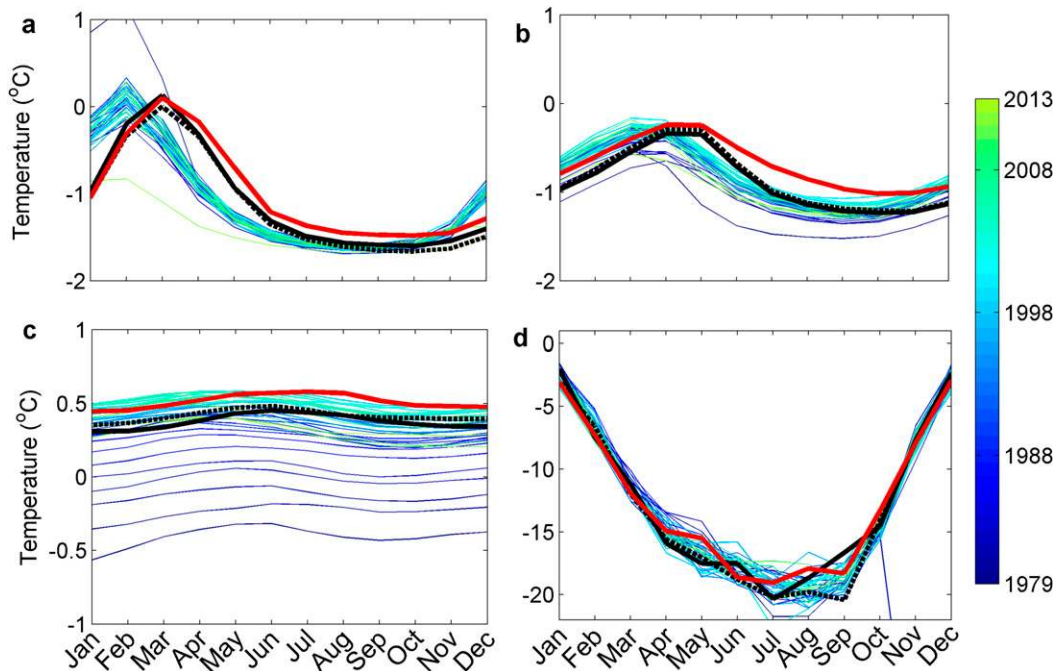


FIG. 9. Average ocean temperatures over the circumpolar region to the south of 60°S. Strong cyclonic wind forcing in 2016 caused overall warmest ocean states at the surface and at 55 and 105-m depths. (a) Average monthly SST. (b) Ocean temperature at the depth of 55 m. (c) Ocean temperature at the depth of 105 m. (d) The 2-m air temperature. The black solid, black dashed, and red solid lines are for 2014, 2015, and 2016 respectively.

forcing induced by direct atmospheric forcing and induced by heat anomalies transported from other regions that are ultimately wind-driven.

The relative contributions of different forcing factors to the differences in monthly total SIEs between 2016 and the corresponding monthly means over 2006–15 are calculated as

$$(\text{SIE}_{\text{ens}} - \text{SIE}_{\text{mean}}) / (\text{SIE}_{2016} - \text{SIE}_{\text{mean}}) \times 100,$$

where SIE_{ens} stands for monthly total SIEs averaged over the 10 ensemble members or 10 years from 2006 to 2015 in an ensemble sensitivity experiment, SIE_{mean} stands for the means of monthly total SIEs over 2006–15 from the control run, and SIE_{2016} stands for monthly total SIEs in 2016 from the control run.

The extremely low monthly SLP during the first three months of 2016 caused unprecedented strong cyclonic wind forcing. Under such strong and persistent forcing, the average SST over the region to the south of 60°S reached the warmest states from April 2016 compared to those of each year during 1979–2015 (Fig. 9). However, the ensemble results from the sensitivity experiments (Fig. 8) indicate that the warm SSTs in 2016 (experiment 2016SST) were only responsible for small portions of the differences between 2016 and the means over 2006–15

(Fig. 8b) (the relative contribution ranges from 5.1% in December to 42.4% in March, and the annual mean is 16.3%). The weak effect of the SSTs on total Antarctic SIE is further confirmed by the weak correlations between the average SSTs in Fig. 9a and total Antarctic SIEs in Fig. 2b for each month over 1979–2016 (see Table 4).

In stark contrast, the full atmospheric forcing in 2016 (experiment 2016ATMOS) and wind forcing only in 2016 (experiment 2016WINDS) make very similar and much larger contributions than the oceanic thermal forcing (Fig. 8). The relative contribution of wind forcing only (experiment 2016WINDS) ranges from 51.1% in August to 91.6% in June, and the annual mean is 66.3% that is very close to the annual mean of 72.1% for experiment 2016ATMOS. These results thus suggest that the wind only forcing played a dominant role in generating the large reductions in total Antarctic SIE in 2016.

The declines of total SIA during April–September 2016 (Fig. 3) were apparently induced by the broad surface warming in the Southern Ocean (Figs. 6 and 9; Stuecker et al. 2017; Meehl et al. 2019) and the persistently strong zonal wavenumber-3 pattern (Fig. 6; Schlosser et al. 2018). Although the declines were small, we suggest that they caused the early occurrence of the

TABLE 4. Correlations (those in bold are statistically significant with the confidence level being greater than 99% by the Monte Carlo method) between monthly total SIEs in Fig. 2b and monthly SSTs averaged over the circumpolar region to the south of 60°S in Fig. 9a.

Month	Jan	Feb	Mar	Apr	May	Jun	Jul	Aug	Sep	Oct	Nov	Dec
Simultaneous	-0.39	-0.37	-0.09	0.23	0.03	-0.15	-0.05	-0.11	-0.14	-0.25	-0.13	-0.05
SST leads by 1 month	-0.54	-0.32	0.21	0.44	0.42	0.30	0.35	-0.04	-0.27	-0.30	-0.46	-0.27
SST lags by 1 month	-0.37	-0.19	-0.07	0.13	0.03	0.01	0.10	-0.15	0.05	0.1	-0.30	0.04

maximum SIE in 2016, which occurred on 28 August as reported in Turner et al. (2017). We suggest that the much faster retreat in spring 2016 was also preconditioned by the effects of atmospheric and oceanic forcing before October 2016, in addition to the most negative SAM in November 2016 since 1968 (Turner et al. 2017; Schlosser et al. 2018).

4. Concluding remarks

As analyzed in this study, the rapid decline of total Antarctic sea ice extent was predominantly a result of record atmospheric low pressure systems over sectors of the Southern Ocean in 2016. Turner et al. (2013) suggested that the record high sea ice extent in 2012 was related to the deep atmospheric lows in the circumpolar trough region since late August 2012. However, the atmospheric forcing conditions in 2016 were extremely unusual in several aspects, manifested by several record low daily and monthly mean sea level pressure values at southern high latitudes in January–March, June, and September 2016 during 1979–2016. These extreme atmospheric conditions were particularly associated with the deepening of Amundsen Sea low, along with the strong and persistent zonal wavenumber-3 pattern during May–August 2016 that was also documented in Schlosser et al. (2018). The resulting strong meridional flows led to enhanced warm and cold advection and strong sea ice drifts. In addition, the resulting extremely strong cyclonic wind forcing generated the warmest sea surface conditions at southern high latitudes during April–October 2016 in the model simulation. The persistent warm sea surface conditions have also been revealed by analyzing observational data (Stuecker et al. 2017; Meehl et al. 2019). Consequently, these atmospheric and oceanic conditions exerted extremely strong and very unusual thermodynamic and dynamic forcing on Antarctic sea ice in 2016.

In 2016, Antarctic sea ice started to retreat in April, as revealed by analyzing the evolution of monthly total sea ice area anomaly, which reflects a more detailed sea ice response to the atmospheric and oceanic forcing than analyzing the total sea ice extent. The sea ice retreat during April–August 2016 contributed to the occurrence of an early maximum total sea ice extent on 28 August in

2016 and preconditioned the occurrences of the record low monthly total sea ice area in September 2016 and record low monthly total sea ice extent in October 2016.

These sea ice responses to the atmospheric and oceanic forcing were well captured by the employed high-resolution global ocean–sea ice model, MITgcm-ECCO2. Such a good fit enables us to quantify the relative roles played by the atmospheric and oceanic forcing and hence identify the major driver for the rapid decline of total Antarctic sea ice extent. Our model results show that both thermal and dynamic effects of the wind anomalies generated large regional positive and negative sea ice concentration anomalies. The wind-driven sea ice drift anomalies were mainly responsible for the rapid decrease in total Antarctic sea ice extent in spring 2016, with the role of the ocean surface warming being minor.

The good fit between the modeled and observed sea ice anomaly patterns and total sea ice extent evolutions substantiate the high qualities of the atmospheric reanalysis data and the employed ocean–sea ice models. These advancements facilitate identifying the major driver of large variability in total Antarctic sea ice extent. Although the tropical forcing has been suggested to contribute to the generation of the atmospheric conditions in 2016 (Stuecker et al. 2017; Wang et al. 2019; Meehl et al. 2019), the identified dominant effects of the wind-driven sea ice drift on total Antarctic sea ice extent urge a more complete understanding of past and future changes in winds, particularly how such extreme atmospheric conditions as in 2016 were established, for enhancing our ability to understand and predict the Antarctic sea ice variability. The dominant wind-driven sea ice drift effects tend to generate larger variability in total sea ice extent in the Antarctic than in the Arctic, as Antarctic sea ice movement is not bounded by continents at lower latitudes. The intensified sea ice drifts in such extreme events also greatly change the freshwater transport patterns, with strong implications for oceanic conditions.

We note that the record-low sea ice extent continued since the end of 2016 after the continuing record-high sea ice extent over 2012–14. This feature raises interesting questions that need to be addressed in the future, such as which processes are responsible for the

sustained record-high sea ice extent over 2012–14 and then the sustained record-low sea ice extent over 2016–18 and how to quantify the relative roles played by these processes compared to that by the wind-driven sea ice drift in large Antarctic sea ice variability. Addressing these questions will offer a more complete understanding of large Antarctic sea ice variability and will be useful for us to predict the transition between the phase with sustained high Antarctic sea ice extents and the phase with sustained low Antarctic sea ice extents.

Acknowledgments. Z. Wang and C. Liu were supported by the Major State Basic Research Development Program of China (2016YFA0601804). Z. Wang was supported by the Global Change Research Program of China (2015CB953900), by the project (41876220) of National Natural Science Foundation of China and by “the Fundamental Research Funds for the Central Universities” (2017B04814, 2017B20714). We thank Dr. Martin Losch (Alfred-Wegener-Institut für Polar- und Meeresforschung, Germany) for his helpful comments on this work. The authors declare no conflicts of interest. The data presented in this article are available from the authors on request.

REFERENCES

- Adcroft, A., J. Campin, C. Hill, and J. Marshall, 2004: Implementation of an atmosphere–ocean general circulation model on the expanded spherical cube. *Mon. Wea. Rev.*, **132**, 2845–2863, <https://doi.org/10.1175/MWR2823.1>.
- Bintanja, R., G. J. van Oldenborgh, S. S. Drijfhout, B. Wouters, and C. A. Katsman, 2013: Important role for ocean warming and increased ice-shelf melt in Antarctic sea-ice expansion. *Nat. Geosci.*, **6**, 376–379, <https://doi.org/10.1038/ngeo1767>.
- Bracegirdle, T. J., and G. J. Marshall, 2012: The reliability of Antarctic tropospheric pressure and temperature in the latest global reanalyses. *J. Climate*, **25**, 7138–7146, <https://doi.org/10.1175/JCLI-D-11-00685.1>.
- Cavaleri, D. J., P. Gloersen, and W. J. Campbell, 1984: Determination of sea ice parameters with the Nimbus-7 SMMR. *J. Geophys. Res.*, **89**, 5355–5369, <https://doi.org/10.1029/JD089iD04p05355>.
- Comiso, J. C., and F. Nishio, 2008: Trends in the sea ice cover using enhanced and compatible AMSR-E, SSM/I, and SMMR data. *J. Geophys. Res.*, **113**, C02S07, <https://doi.org/10.1029/2007JC004257>.
- Dee, D. P., and Coauthors, 2011: The ERA-Interim reanalysis: Configuration and performance of the data assimilation system. *Quart. J. Roy. Meteor. Soc.*, **137**, 553–597, <https://doi.org/10.1002/qj.828>.
- Doddridge, E. W., and J. Marshall, 2017: Modulation of the seasonal cycle of Antarctic sea ice extent related to the Southern Annular Mode. *Geophys. Res. Lett.*, **44**, 9761–9768, <https://doi.org/10.1002/2017GL074319>.
- Fetterer, F., K. Knowles, W. Meier, and M. Savoie, 2017: Sea ice index, version 3. National Snow and Ice Data Center, digital media, <https://nsidc.org/data/g02135>.
- Godfred-Spenning, C. R., and I. Simmonds, 1996: An analysis of Antarctic sea-ice and extratropical cyclone associations. *Int. J. Climatol.*, **16**, 1315–1332, [https://doi.org/10.1002/\(SICI\)1097-0088\(199612\)16:12<1315::AID-JOC92>3.0.CO;2-M](https://doi.org/10.1002/(SICI)1097-0088(199612)16:12<1315::AID-JOC92>3.0.CO;2-M).
- Goosse, H., and V. Zunz, 2014: Decadal trends in the Antarctic sea ice extent ultimately controlled by ice–ocean feedback. *Cryosphere*, **8**, 453–470, <https://doi.org/10.5194/tc-8-453-2014>.
- , W. Lefebvre, A. de Montety, E. Crespin, and A. Orsi, 2009: Consistent past half-century trends in the atmosphere, the sea ice and the ocean at high southern latitudes. *Climate Dyn.*, **33**, 999–1016, <https://doi.org/10.1007/s00382-008-0500-9>.
- Guemas, V., F. Doblas-Reyes, A. Germe, M. Chevallier, and D. Salas y Mélia, 2013: September 2012 Arctic sea ice minimum: Discriminating between sea ice memory, the August 2012 extreme storm, and prevailing warm conditions [in “Explaining Extreme Events of 2012 from a Climate Perspective”]. *Bull. Amer. Meteor. Soc.*, **94**, S20–S22, <https://doi.org/10.1175/BAMS-D-13-00085.1>.
- Haid, V., D. Iovino, and S. Masina, 2017: Impacts of freshwater changes on Antarctic sea ice in an eddy-permitting sea-ice–ocean model. *Cryosphere*, **11**, 1387–1402, <https://doi.org/10.5194/tc-11-1387-2017>.
- Holland, M. M., E. Blanchard-Wrigglesworth, J. Kay, and S. Vavrus, 2013: Initial-value predictability of Antarctic sea ice in the community climate system model 3. *Geophys. Res. Lett.*, **40**, 2121–2124, <https://doi.org/10.1002/grl.50410>.
- Holland, P. R., 2014: The seasonality of Antarctic sea ice trends. *Geophys. Res. Lett.*, **41**, 4230–4237, <https://doi.org/10.1002/2014GL060172>.
- , and R. Kwok, 2012: Wind-driven trends in Antarctic sea-ice drift. *Nat. Geosci.*, **5**, 872–875, <https://doi.org/10.1038/ngeo1627>.
- Hosking, J. S., A. Orr, G. J. Marshall, J. Turner, and T. Phillips, 2013: The influence of the Amundsen-Bellinghousen Seas low on the climate of West Antarctica and its representation in coupled climate model simulations. *J. Climate*, **26**, 6633–6648, <https://doi.org/10.1175/JCLI-D-12-00813.1>.
- Kanamitsu, M., W. Ebisuzaki, J. Woollen, S. Yang, J. J. Hnilo, M. Fiorino, and G. L. Potter, 2002: NCEP–DOE AMIP-II Reanalysis (R-2). *Bull. Amer. Meteor. Soc.*, **83**, 1631–1643, <https://doi.org/10.1175/BAMS-83-11-1631>.
- Kimura, N., 2004: Sea ice motion in response to surface wind and ocean current in the Southern Ocean. *J. Meteor. Soc. Japan*, **82**, 1223–1231, <https://doi.org/10.2151/jmsj.2004.1223>.
- , and M. Wakatsuchi, 2011: Large-scale processes governing the seasonal variability of the Antarctic sea ice. *Tellus*, **63A**, 828–840, <https://doi.org/10.1111/j.1600-0870.2011.00526.x>.
- Kohyama, T., and D. L. Hartmann, 2016: Antarctic sea ice response to weather and climate modes of variability. *J. Climate*, **29**, 721–741, <https://doi.org/10.1175/JCLI-D-15-0301.1>.
- Kottmeier, C., J. Olf, W. Frieden, and R. Roth, 1992: Wind forcing and ice motion in the Weddell Sea region. *J. Geophys. Res.*, **97**, 20 373–20 383, <https://doi.org/10.1029/92JD02171>.
- Kusahara, K., P. Reid, G. D. Williams, R. Massom, and H. Hasumi, 2018: An ocean–sea ice model study of the unprecedented Antarctic sea ice minimum in 2016. *Environ. Res. Lett.*, **13**, 084020, <https://doi.org/10.1088/1748-9326/aad624>.
- Lefebvre, W., and H. Goosse, 2005: Influence of the Southern Annular Mode on the sea ice–ocean system: The role of the thermal and mechanical forcing. *Ocean Sci.*, **1**, 145–157, <https://doi.org/10.5194/os-1-145-2005>.
- Liu, J. P., J. A. Curry, and D. G. Martinson, 2004: Interpretation of recent Antarctic sea ice variability. *Geophys. Res. Lett.*, **31**, L02205, <https://doi.org/10.1029/2003G1018732>.

- Losch, M., D. Menemenlis, J.-M. Campin, P. Heimbach, and C. Hill, 2010: On the formulation of sea-ice models. Part 1: Effects of different solver implementations and parameterizations. *Ocean Modell.*, **33**, 129–144, <https://doi.org/10.1016/j.ocemod.2009.12.008>.
- Marshall, J., A. Adcroft, C. Hill, L. Perelman, and C. Heisey, 1997a: A finite-volume, incompressible Navier Stokes model for studies of the ocean on parallel computers. *J. Geophys. Res.*, **102**, 5753–5766, <https://doi.org/10.1029/96JC02775>.
- , C. Hill, L. Perelman, and A. Adcroft, 1997b: Hydrostatic, quasi-hydrostatic, and nonhydrostatic ocean modeling. *J. Geophys. Res.*, **102**, 5733–5752, <https://doi.org/10.1029/96JC02776>.
- Marsland, S. J., and J. O. Wolff, 2001: On the sensitivity of Southern Ocean sea ice to the surface freshwater flux: A model study. *J. Geophys. Res.*, **106**, 2723–2741, <https://doi.org/10.1029/2000JC900086>.
- Martinson, D. G., 1990: Evolution of the Southern Ocean winter mixed layer and sea ice: Open ocean deep-water formation and ventilation. *J. Geophys. Res.*, **95**, 11 641–11 654, <https://doi.org/10.1029/JC095iC07p11641>.
- Massonnet, F., V. Guemas, N. S. Fuckar, and F. J. Doblas-Reyes, 2015: The 2014 high record of Antarctic sea ice extent [in “Explaining Extremes of 2014 from a Climate Perspective”]. *Bull. Amer. Meteor. Soc.*, **96** (12), S163–S167, <https://doi.org/10.1175/BAMS-D-15-00093.1>.
- Meehl, G. A., and Coauthors, 2019: Sustained ocean changes contributed to sudden Antarctic sea ice retreat in late 2016. *Nat. Commun.*, **10**, 14, <https://doi.org/10.1038/S41467-018-07865-9>.
- Menemenlis, D., J.-M. Campin, P. Heimbach, C. Hill, T. Lee, A. Nguyen, M. Schodlok, and H. Zhang, 2008: ECCO2: High resolution global ocean and sea ice data synthesis. *Mercator Ocean Quart. Newsletter*, **31**, 13–21.
- Parkinson, C. L., and D. J. Cavalieri, 2012: Antarctic sea ice variability and trends, 1979–2010. *Cryosphere*, **6**, 871–880, <https://doi.org/10.5194/tc-6-871-2012>.
- , and J. C. Comiso, 2013: On the 2012 record low Arctic sea ice cover: Combined impact of preconditioning and an August storm. *Geophys. Res. Lett.*, **40**, 1356–1361, <https://doi.org/10.1002/grl.50349>.
- Raphael, M. N., 2007: The influence of atmospheric zonal wave three on Antarctic sea ice variability. *J. Geophys. Res.*, **112**, D12112, <https://doi.org/10.1029/2006JD007852>.
- Reid, P., S. Stammerjohn, R. Massom, T. Scambos, and J. Lieser, 2015: The record 2013 Southern Hemisphere sea-ice extent maximum. *Ann. Glaciol.*, **56**, 99–106, <https://doi.org/10.3189/2015AoG69A892>.
- Reynolds, R. W., N. A. Rayner, T. M. Smith, D. C. Stokes, and W. Wang, 2002: An improved in situ and satellite SST analysis for climate. *J. Climate*, **15**, 1609–1625, [https://doi.org/10.1175/1520-0442\(2002\)015<1609:AIISAS>2.0.CO;2](https://doi.org/10.1175/1520-0442(2002)015<1609:AIISAS>2.0.CO;2).
- Schlosser, E., F. A. Haumann, and M. N. Raphael, 2018: Atmospheric influences on the anomalous 2016 Antarctic sea ice decay. *Cryosphere*, **12**, 1103–1119, <https://doi.org/10.5194/tc-12-1103-2018>.
- Simmonds, I., and T. H. Jacka, 1995: Relationship between the interannual variability of Antarctic sea ice and the Southern Oscillation index. *J. Climate*, **8**, 637–647, [https://doi.org/10.1175/1520-0442\(1995\)008<0637:RBTIVO>2.0.CO;2](https://doi.org/10.1175/1520-0442(1995)008<0637:RBTIVO>2.0.CO;2).
- Simpkins, G. R., L. M. Ciasto, D. W. Thompson, and M. H. England, 2012: Seasonal relationships between large-scale climate variability and Antarctic sea ice concentration. *J. Climate*, **25**, 5451–5469, <https://doi.org/10.1175/JCLI-D-11-00367.1>.
- Stammerjohn, S. E., D. G. Martinson, R. C. Smith, X. Yuan, and D. Rind, 2008: Trends in Antarctic annual sea ice retreat and advance and their relation to El Niño–Southern Oscillation and Southern Annular Mode variability. *J. Geophys. Res.*, **113**, C03S90, <https://doi.org/10.1029/2007JC004269>.
- , R. Massom, D. Rind, and D. Martinson, 2012: Regions of rapid sea ice change: An inter-hemispheric seasonal comparison. *Geophys. Res. Lett.*, **39**, L06501, <https://doi.org/10.1029/2012GL050874>.
- Stuecker, M. F., C. M. Bitz, and K. C. Armour, 2017: Conditions leading to the unprecedented low Antarctic sea ice extent during the 2016 austral spring season. *Geophys. Res. Lett.*, **44**, 9008–9019, <https://doi.org/10.1002/2017GL074691>.
- Swart, N. C., and J. C. Fyfe, 2013: The influence of recent Antarctic ice sheet retreat on simulated sea ice area trends. *Geophys. Res. Lett.*, **40**, 4328–4332, <https://doi.org/10.1002/grl.50820>.
- Turner, J., and Coauthors, 2009: Non-annular atmospheric circulation change induced by stratospheric ozone depletion and its role in the recent increase of Antarctic sea ice extent. *Geophys. Res. Lett.*, **36**, L08502, <https://doi.org/10.1029/2009GL037524>.
- , J. S. Hosking, T. Phillips, and G. J. Marshall, 2013: Temporal and spatial evolution of the Antarctic sea ice prior to the September 2012 record maximum extent. *Geophys. Res. Lett.*, **40**, 5894–5898, <https://doi.org/10.1002/2013GL058371>.
- , T. Phillips, G. J. Marshall, J. S. Hosking, J. O. Pope, T. J. Bracegirdle, and P. Deb, 2017: Unprecedented springtime retreat of Antarctic sea ice in 2016. *Geophys. Res. Lett.*, **44**, 6868–6875, <https://doi.org/10.1002/2017GL073656>.
- Venables, H. J., and M. P. Meredith, 2014: Feedbacks between ice cover, ocean stratification, and heat content in Ryder Bay, western Antarctic peninsula. *J. Geophys. Res. Oceans*, **119**, 5323–5336, <https://doi.org/10.1002/2013JC009669>.
- Wang, G., H. H. Hendon, J. M. Arblaster, E.-P. Lim, S. Abhik, and P. van Rensch, 2019: Compounding tropical and stratospheric forcing of the record low Antarctic sea-ice in 2016. *Nat. Commun.*, **10**, 13, <https://doi.org/10.1038/S41467-018-07689-7>.
- Wang, Z., J. Turner, B. Sun, B. Li, and C. Liu, 2014: Cyclone-induced rapid creation of extreme Antarctic sea ice conditions. *Sci. Rep.*, **4**, 5317, <https://doi.org/10.1038/srep05317>.
- , X. Zhang, Z. Guan, B. Sun, X. Yang, and C. Liu, 2015: An atmospheric origin of the multi-decadal bipolar seesaw. *Sci. Rep.*, **5**, 8909, <https://doi.org/10.1038/srep08909>.
- Zhang, J., 2007: Increasing Antarctic sea ice under warming atmospheric and oceanic conditions. *J. Climate*, **20**, 2515–2529, <https://doi.org/10.1175/JCLI4136.1>.
- Zwally, H. J., J. C. Comiso, C. L. Parkinson, D. J. Cavalieri, and P. Gloersen, 2002: Variability of Antarctic sea ice 1979–1998. *J. Geophys. Res.*, **107**, 3041, <https://doi.org/10.1029/2000JC000733>.